REPORT No. 563

CALCULATED AND MEASURED PRESSURE DISTRIBUTIONS OVER THE MIDSPAN SECTION OF THE N. A. C. A. 4412 AIRFOIL

By Robert M. Pinkerton

SUMMARY

Pressures were simultaneously measured in the variable-density tunnel at 54 orifices distributed over the midspan section of a 5- by 30-inch rectangular model of the N. A. C. A. 4412 airfoil at 17 angles of attack ranging from −20° to 30° at a Reynolds Number of approximately 3,000,000. Accurate data were thus obtained for studying the deviations of the results of potential-flow theory from measured results. The results of the analysis and a discussion of the experimental technique are presented.

It is shown that theoretical calculations made either at the effective angle of attack or at a given actual lift do not accurately describe the observed pressure distribution over an airfoil section. There is therefore developed a modified theoretical calculation that agrees reasonably well with the measured results of the tests of the N. A. C. A. 4412 section and that consists of making the calculations and evaluating the circulation by means of the experimentally obtained lift at the effective angle of attack; i. e., the angle that the chord of the model makes with the direction of the flow in the region of the section under consideration. In the course of the computations the shape parameter ϵ is modified, thus leading to a modified or an effective profile shape that differs slightly from the specified shape.

INTRODUCTION

Pressure-distribution measurements over an airfoil section provide, directly, the knowledge of the air-force distribution along the chord that is required for some purposes. In addition, such data, when compared with the results of potential-flow (nonviscous fluid) theory, provide a means of studying the effects of viscous forces on the flow about the airfoil section.

The results of experimental pressure measurements for a few miscellaneous airfoils may be found in various publications. The general application of this method of obtaining design data, however, is limited because of the expense of making such measurements.

A method of calculating the pressure distribution is developed in references 1 and 2. This method, based on the "ideal fluid" or potential-flow theory, gives the local velocities over the surface; the pressures are calculated by means of Bernoulli's equation. Although this method provides an inexpensive means of obtaining the distribution of pressure, the results may not be in satisfactory agreement with measured results. Such disagreement, however, is not surprising since the theory does not account for the effects of the viscous boundary layer.

A reasonably accurate method of calculating the pressure distribution over an airfoil section is desirable and might be obtained by two procedures. First, such a method might be found by the development of a complete theory. Such a theory, however, must take into account all the factors or phenomena involved and must give satisfactory agreement with actual measurement. A second procedure, the most feasible one at present, is the development of a rational method of correcting the application of the potential-flow theory to minimize the discrepancies between the theoretical and measured results.

It was realized, however, that unusually reliable experimental pressure-distribution data for comparison with calculations were not available. The experiments to obtain such data consisted of pressure measurements at a large number of points around one section of an airfoil. Because the investigation was primarily intended to study deviations of the actual from the ideal, or potential, flow, the tests were made in the variable-density tunnel over a range of values of the Reynolds Number, representing varying effects of viscosity. In addition, tests were made in the 24-inch high-speed tunnel at certain corresponding values of the Reynolds Number obtained by means of high speeds, thereby bringing out the effects of compressibility. Parts of this experimental investigation outside the scope of this report are still incomplete.

The present report, which presents the most important of the experimental results (those corresponding to the highest value of the Reynolds Number), is divided into two parts. The first part comprises the description and discussion of the experimental technique: Materials that are essential to establish the fact that the measured results are sufficiently accurate and reliable to meet the demands of the subsequent analysis. The

second part presents a comparison of theoretically calculated results with measured results and an analysis of the differences and probable causes. A method is developed to modify the application of potential-flow theory in order to minimize discrepancies from the measured pressure distributions.

EXPERIMENTAL PRESSURE DISTRIBUTION

APPARATUS AND TESTS

The experimental investigation described herein was made in the variable-density wind tunnel (reference 3). The model used was a standard duralumin airfoil having

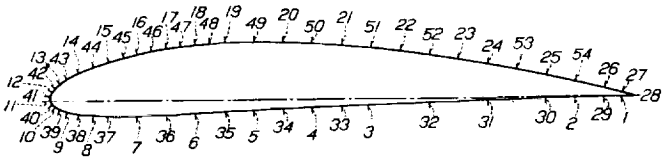

FIGURE 1.—Distribution of pressure orifices about the N. A. C. A. 4412 airfoil.

the N. A. C. A. 4412 section and a rectangular plan form with a span of 30 inches and a chord of 5 inches. It was modified by replacing a midspan section 1 inch in length with a brass section in which the pressure orifices were located. The 54 orifices, each 0.008 inch in diameter, were drilled perpendicularly into the airfoil surface and placed in 2 rows about the airfoil. The method and accuracy of construction of the model are described in reference 3. In order to evaluate the pressure force parallel to the chord, a relatively large number of orifices were located at the nose of the airfoil (fig. 1); well-defined distributions of pressure along a normal to the chord were thus assured. The locations of the pressure orifices are included in table I. Brass tubes were connected to the orifices and carried in grooves in the lower surface of the airfoil to the planes of the supporting struts where they were brought out of the model. After the model was assembled, the grooves were covered with a plate carefully faired into the surface. The tubing extended through the tunnel wall into the dead-air space and the part exposed to the air stream together with the support struts was faired into a single unit (fig. 2). The tubes were connected by rubber tubing to a photorecording multiple-tube manometer mounted in the dead-air space.

Figure 3 shows the 60-tube manometer, composed of 30-inch glass tubes arranged in a semicircle and connected at the lower ends to a common reservoir. The total-head pressure of the air stream was chosen as the reference pressure and was measured by a pitot head, mounted as shown in figure 2, to which four equally spaced manometer tubes were connected. The dynamic pressure of the air stream was determined by two tubes connected to the calibrated static-pressure orifices used in the normal operation of the tunnel. One tube was connected to a set of four orifices spaced around the inner wall of the return passage and the other tube to a set of four orifices spaced around the entrance cone near the test section. The remaining 54 tubes, used to measure the pressure at the orifices on the airfoil, were connected to the tubes leading to the airfoil model.

A lighttight box mounted on the flat side of the semicircle contained drums for holding photostat paper and the necessary operating mechanism. The manometer was arranged so that it could be operated from outside the tank that houses the tunnel.

The manometer characteristics determined by trial included the time required for the meniscuses to become steady and the proper exposure of the photostat paper.

A record of the heights of the manometer fluid in the glass tubes was taken at each of 17 angles of attack

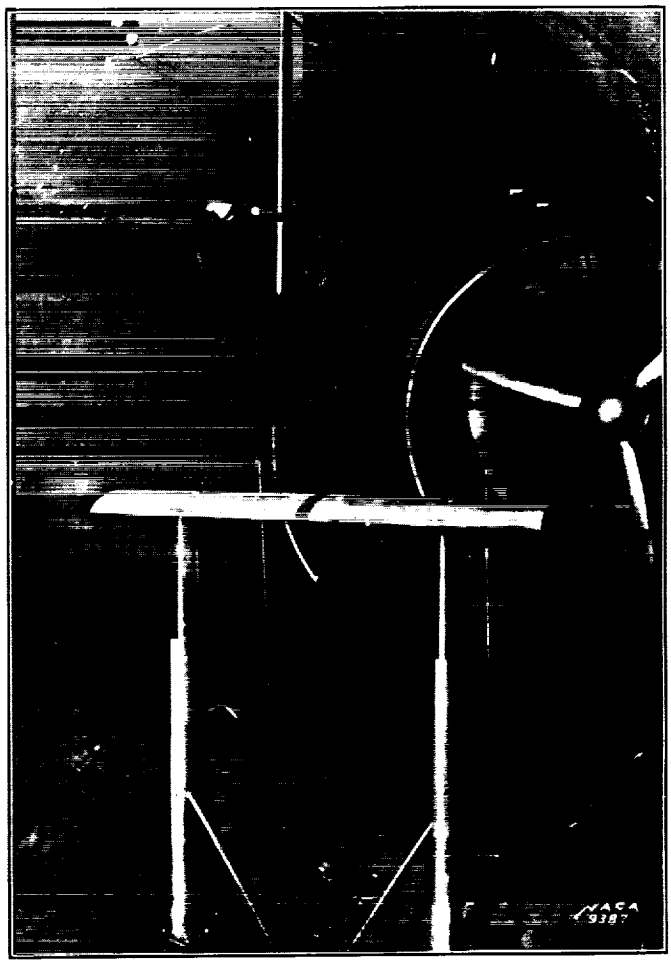

FIGURE 2.—Pressure-distribution model mounted in the tunnel.

from $-20°$ to $30°$ at a Reynolds Number of approximately 3,000,000.

In order to keep the results as accurate as possible, it was necessary to obtain large deflections of the manometer liquids, which was accomplished by using two liquids of widely different specific gravities.

Liquid:	*Specific gravity*
Mercury	13. 6
Tetrabromoethane	3. 0

The proper choice of the angle-of-attack groups and of the liquid enabled the use of large and comparable

deflections throughout the angle-of-attack range. Repeat tests, using the same and different manometer liquids, provided data on the precision of the tests.

RESULTS

A copy of a sample photostat record is shown in figure 4. The pressures in inches of manometer fluid were measured to 0.01 inch. All measurements were made from a reference line obtained by drawing a line connecting the meniscuses of the four reference tubes. The quantities thus obtained from the photostat records were:

$$\Delta p = H - p$$

where H is the total-head pressure of the stream and p, the pressure at the airfoil orifice; and

$$q = \text{factor} \times \Delta p_s$$

where q is the dynamic pressure and Δp_s is the difference in pressure between the static-pressure orifices in the entrance cone and those in the return passage. The factor was previously determined by comparing values of Δp_s with simultaneous values of the dynamic pressure obtained with a calibrated pitot-static tube mounted in the air stream in the absence of a model. Finally, the pressures on the airfoil were computed as ratios to the dynamic pressure, thereby making the results independent of manometer liquid.

Bernoulli's equation for the undisturbed stream becomes

$$p_\infty + \tfrac{1}{2}\rho V^2 = H$$

where p_∞ is the pressure and V the velocity. The pressure of the fluid at the wing orifice is given by

$$p = H - \Delta p$$

Substitute for H from the previous equation and remember that $\tfrac{1}{2}\rho V^2 = q$, the dynamic pressure, then

$$p = p_\infty + q - \Delta p$$

Consider p_∞ as the datum pressure. The pressure coefficient then becomes

$$P = \frac{p - p_\infty}{q} = 1 - \frac{\Delta p}{q}$$

where Δp and q are quantities obtained from the photostat records as previously described. Values of P at each orifice on the airfoil and for all angles of attack are tabulated in table I.

Figure 5 (a, b, c) presents plots of P against orifice position along the chord and against position perpendicular to the chord for each angle of attack. Large-scale plots similar to those presented here were mechanically integrated to obtain the normal-force, the chord-force, and the pitching-moment coefficients, which are defined by the following expressions:

$$c_n = \frac{1}{c}\int P\,dx$$

$$c_c = \frac{1}{c}\int P\,dy$$

$$c_{m_{c/4}} = \frac{1}{c^2}\left[\int P\left(\frac{c}{4} - x\right)dx + \int P y\,dy\right]$$

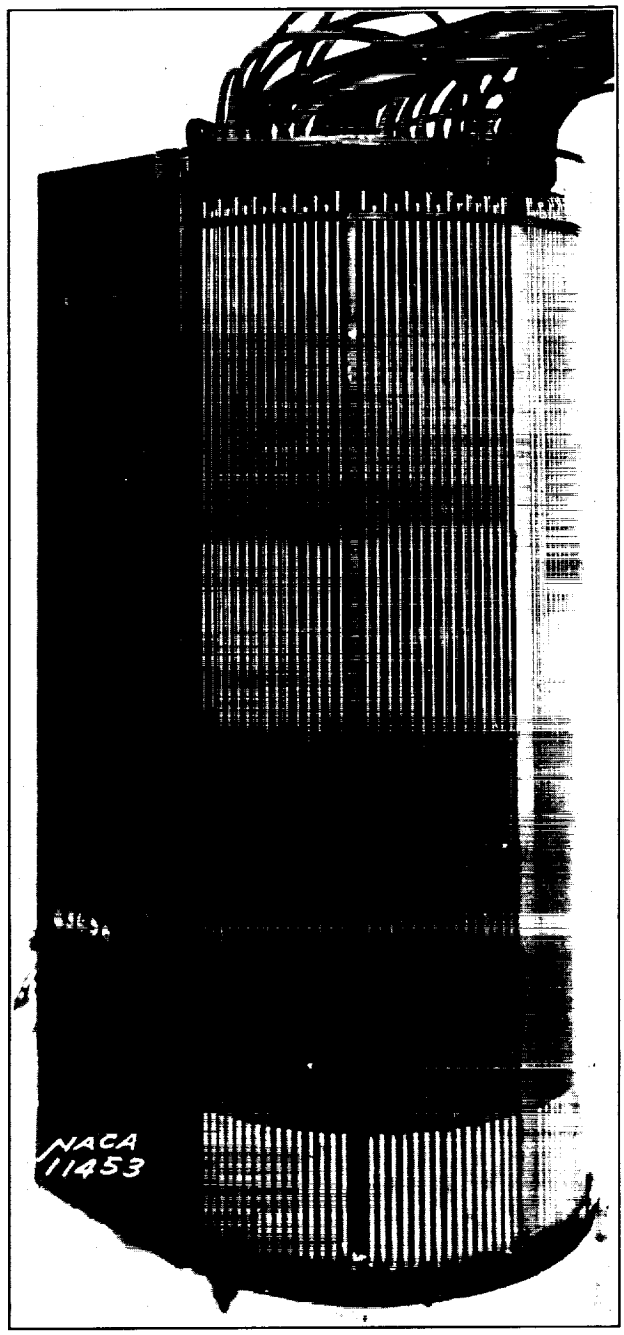

FIGURE 3.—Photorecording multiple-tube manometer.

where c is the chord, x is the orifice station along the chord, and y is the orifice ordinate measured from the chord. The lower-case symbols c_n, c_c, $c_{m_{c/4}}$ designate

section characteristics and refer respectively to the normal-force, chord-force, and pitching-moment coefficients for the midspan section of the airfoil. Plots of these coefficients (see table II) against geometric angle of attack are given in figure 6. The geometric angle of attack α is measured from the mean direction of the flow in the tunnel. This direction is defined as the zero-lift direction of a symmetrical airfoil in the tunnel and was found to be equivalent to 20′ of upflow. In order to have true section characteristics (2-dimensional) for comparison with theoretical calculations, a determination must be made of the effective angle of attack, i. e., the angle that the chord of the model makes with the direction of flow in the region of the midspan section of the model.

The effective angle of attack, corresponding to the angle for 2-dimensional flow, is given by

$$\alpha_0=\alpha-\alpha_i$$

where α_i is the angle that the flow in the region of the airfoil section makes with the direction of the undisturbed flow. The amount of this deviation is small and can be calculated from

$$\alpha_i=\frac{w}{V}$$

where w is the induced normal velocity produced by the vortex system of the airfoil, including the tunnel-wall interference, and V is the velocity of the undisturbed flow. In order to calculate the induced velocity w, the distribution of the lift (or circulation) along the span of the airfoil must be determined. A theoretical method of obtaining this distribution is given in reference 4 and, when applied to this problem, gives for the induced angle of attack of the midspan section

$$\alpha_i=1.584\ c_l$$

where c_l is the lift coefficient for the midspan section. This lift coefficient is obtained from the pressure measurements by means of the equation

$$c_l=c_n\cos\alpha-c_c\sin\alpha$$

Values of c_l, α_i, and α_0 are given in table II.

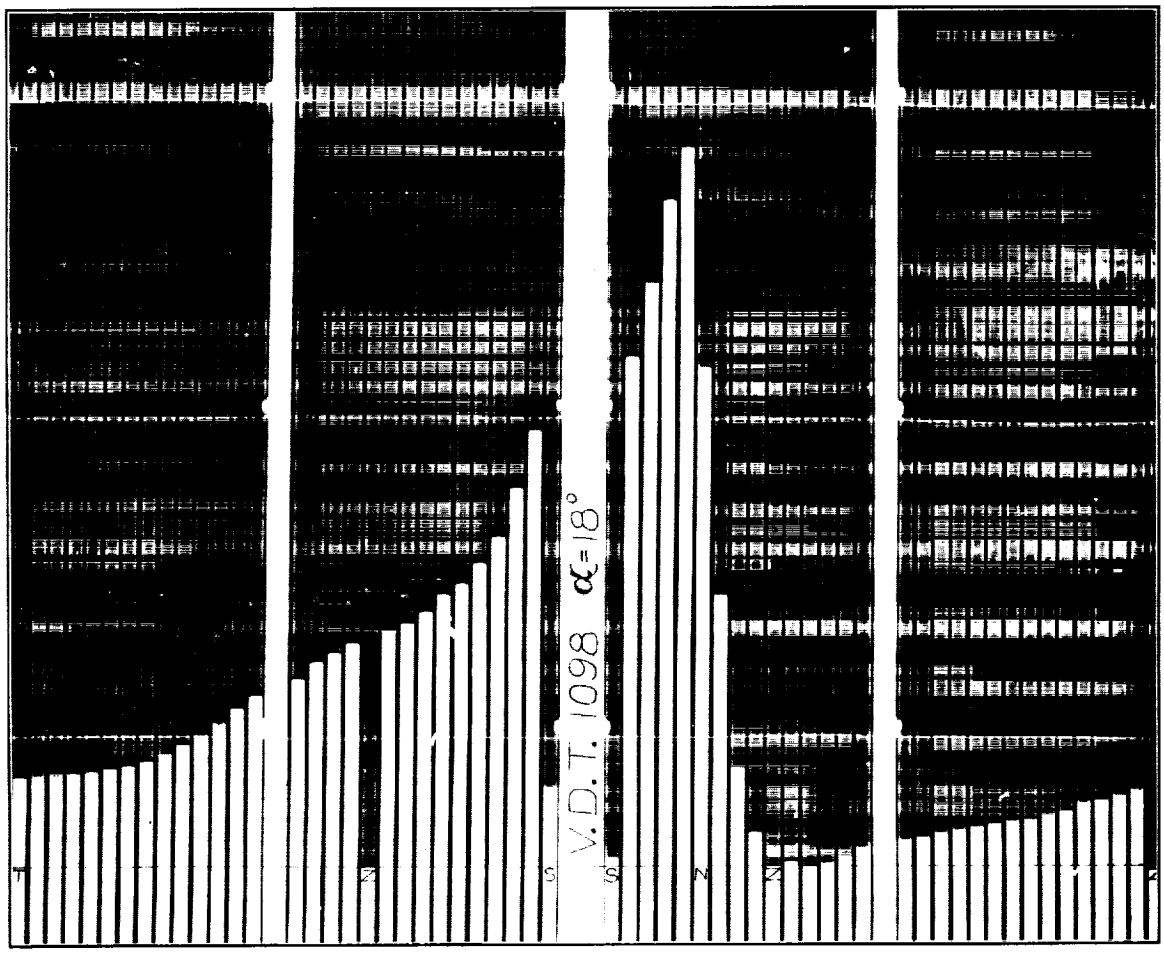

FIGURE 4.—Copy of sample record. N, leading-edge orifice tube; S, static-pressure tubes; T, trailing-edge orifice tube; and Z, reference-pressure tubes.

PRECISION

The reliability of the results of the pressure measurements reported herein may be determined by consideration of the technique of obtaining and measuring the pressure records, of the deviations of the pressure diagrams obtained from several tests at the same angle of attack, and of the method of calculating the effective angle of attack.

The method of obtaining the pressure records is a direct, simultaneous, photographic recording of the height of the liquid in the manometer tubes. Since the pressure coefficients used in the analysis are ratios of quantities taken from the same record, the primary source of error therefore lies in the unequal damping in the tubes connecting the airfoil orifices to the manometer. This source of error was minimized by determining the time required for the liquid in all the tubes to become steady and by delaying the taking of the record at each angle of attack until sufficient time had elapsed. As a further check, a zero record was taken at the end of each test run under the same conditions. In addition, the tubes were checked for leaks before and after each run. In order to minimize any possible error in reading the photostatic records (fig. 4) measurements of the recorded pressures were made independently by two persons. The readings were then com-

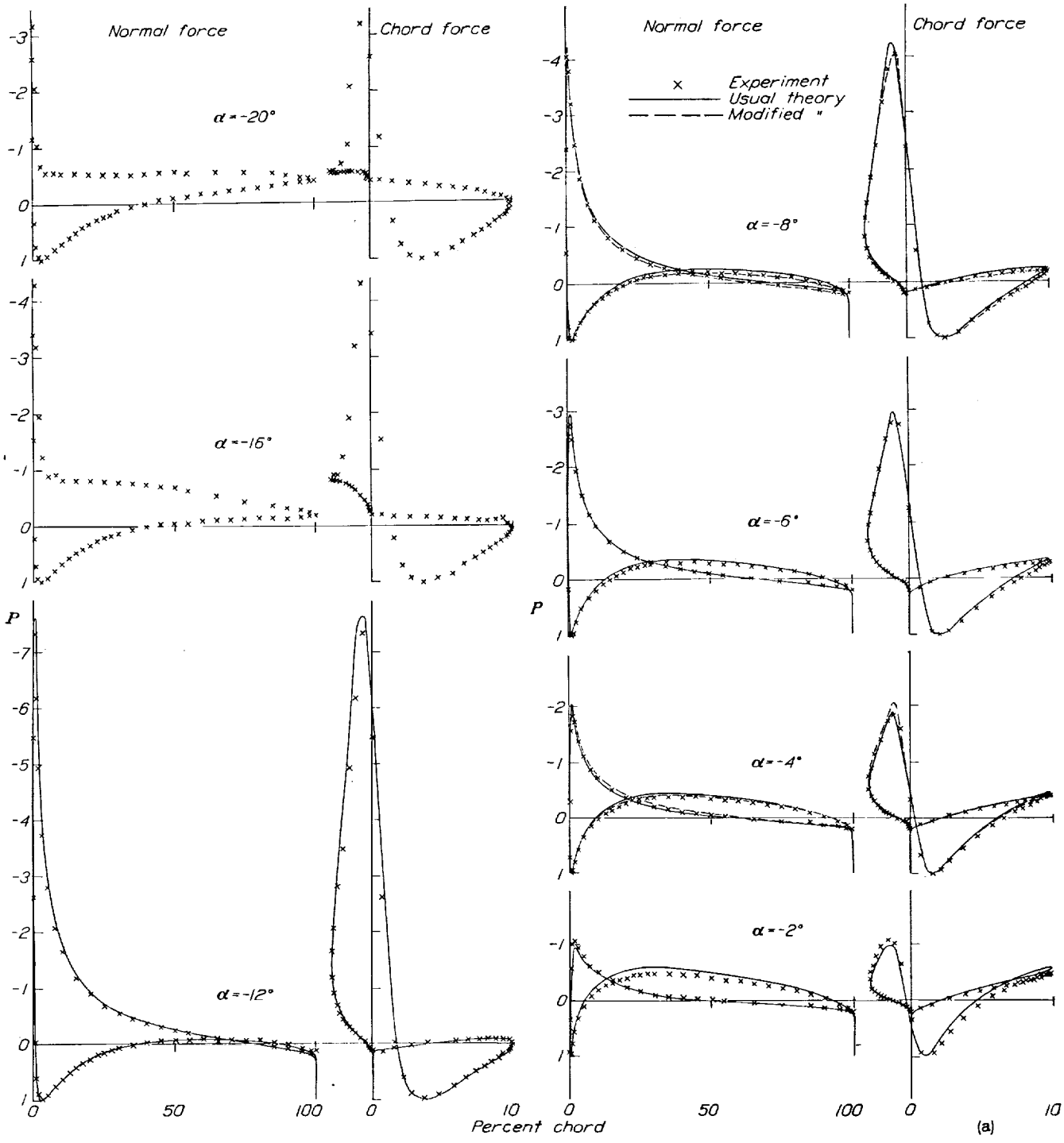

FIGURE 5a.—Experimental and theoretical pressure-distribution diagrams for the N. A. C. A. 4412 airfoil at several angles of attack.

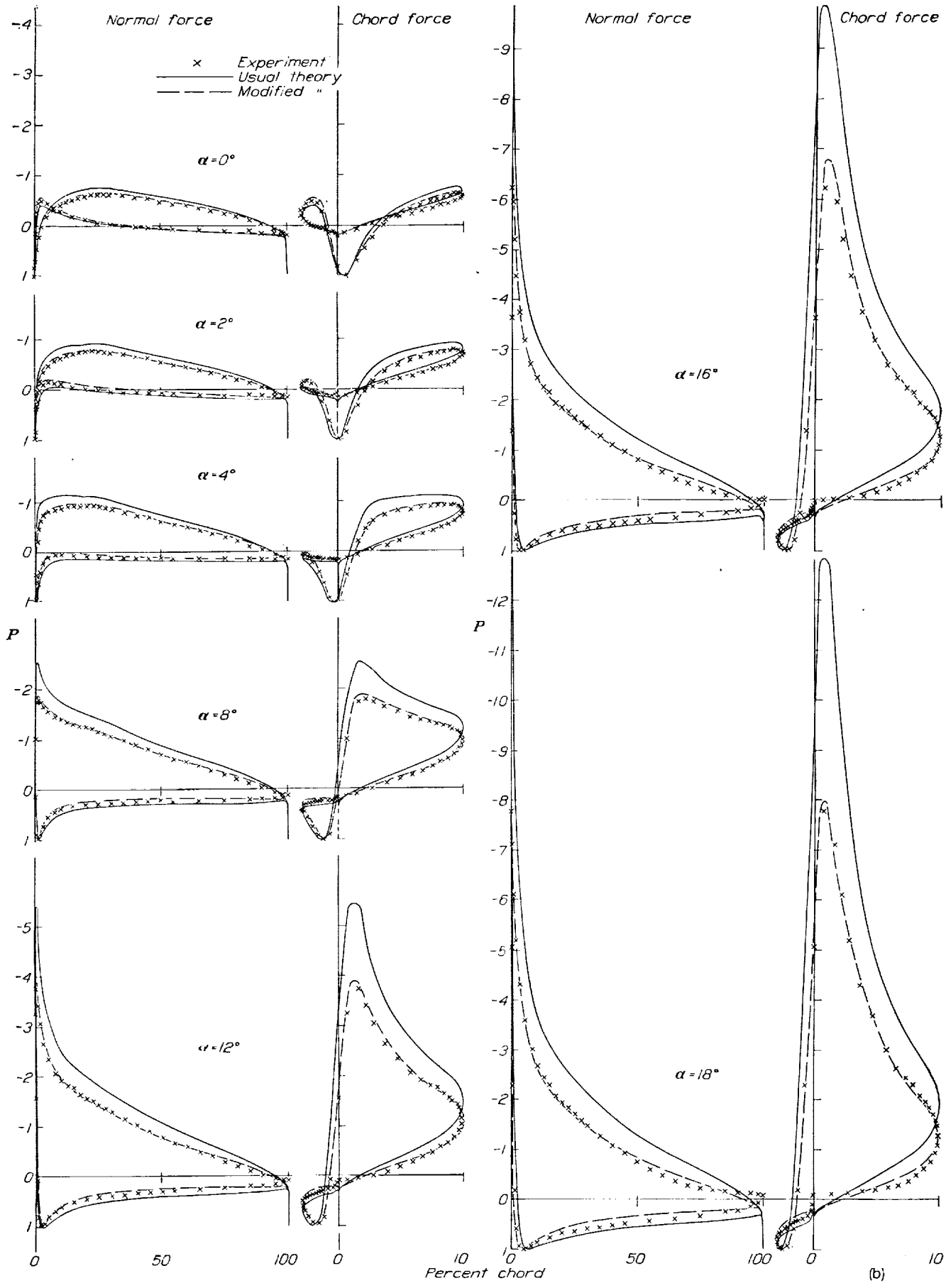

FIGURE 5b.—Experimental and theoretical pressure-distribution diagrams for the N. A. C. A. 4412 airfoil at several angles of attack.

pared and a compromise was made where differences occurred. The differences between any two such independent readings rarely exceeded 0.01 inch except in the case of obvious errors. Possible errors due to shrinkage of the records were avoided by the use of the ratio of two pressures obtained from the same record; namely, the ratio of the pressure at a wing orifice to the dynamic pressure.

The precision of the measured results is indicated by the variations of the pressure diagrams obtained from several tests at the same angle of attack. Figure 7 presents such diagrams at two angles of attack, −4° and 8°. Tetrabromoethane, because of the larger deflections, gave more accurate results, which agreed very closely with the mean values obtained from repeated mercury tests, of which the greatest deviation from the mean values was approximately ±3 percent of the dynamic pressure. This deviation is not a random scattering of points from any given test but is a consistent difference between repeat tests and may

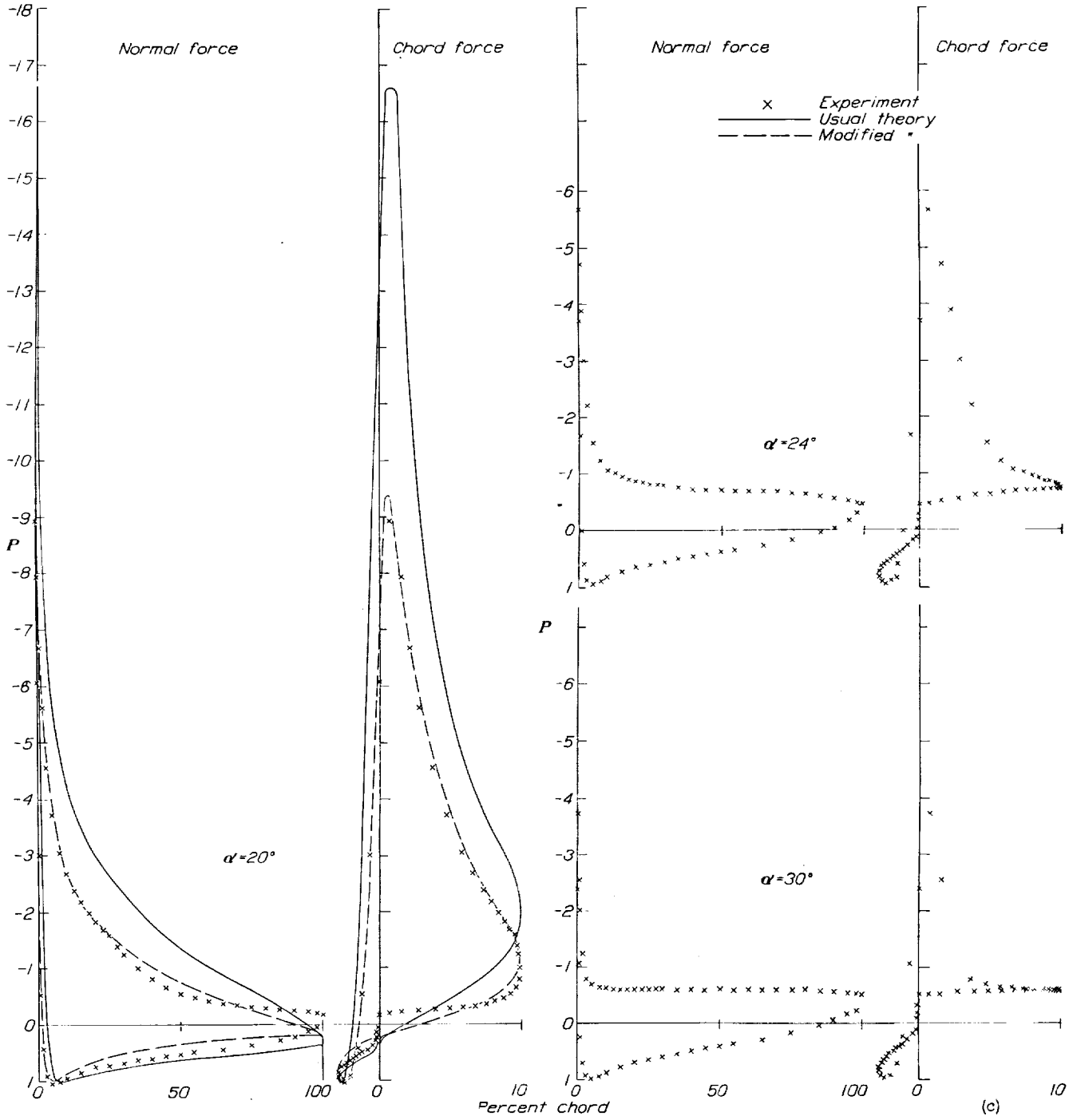

FIGURE 5c.—Experimental and theoretical pressure-distribution diagrams for the N. A. C. A. 4412 airfoil at several angles of attack.

be partly accounted for by a possible small difference in angle of attack. Figure 7 (b) also includes the results of tests made before and after carefully polishing the midspan section of the model. The change in surface smoothness and a slight change in fairness had no discernible effect on the distribution; the differences were

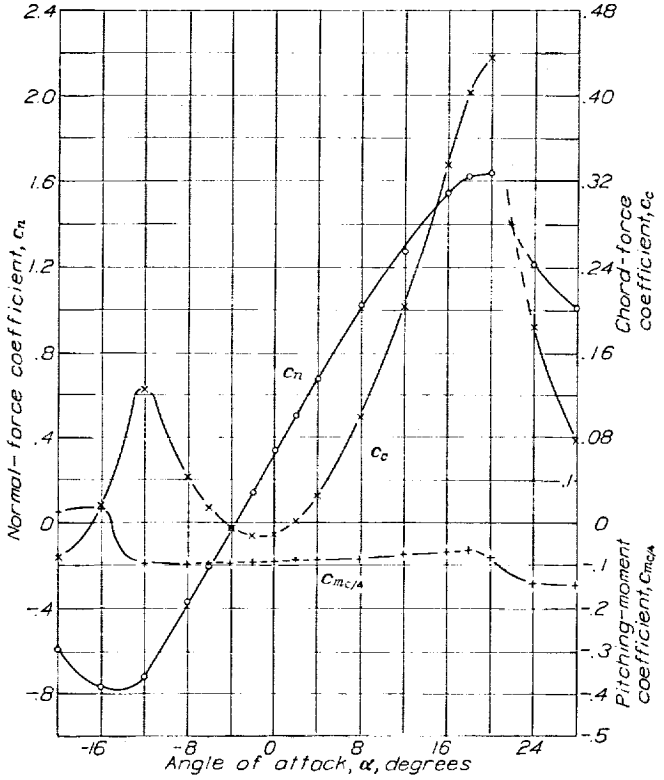

FIGURE 6.—Normal- and chord-force coefficients, and pitching-moment coefficients about the quarter-chord point. The numerical value of c_c should be prefixed by a minus sign.

less than those obtained by repeat tests of the same surface.

The determination of the effective angle of attack of the midspan section entails certain assumptions that are subject to considerable uncertainty. First, the angle of attack of this section may be in error because of the assumption that the deviation of the air-stream axis from the tunnel axis is uniform along the span of the model; i. e., that the geometric angle of attack α is the same for all sections along the span. Actually there is some variation of the air-stream direction across the tunnel. Because of the interference of the support struts, the deflection of the stream in this region might reasonably be expected to exceed the deflection at the midspan section; hence, the deflection at the midspan section is probably less than the effective mean value. Furthermore, a zero deflection of the stream at the midspan section would bring the angle of zero lift obtained from the pressure tests into agreement with force-test results.

A second and rather large source of error lies in the determination of the induced angle of attack. The method used probably produces erroneous results because of the fact that the tips of a rectangular wing carry a larger proportion of the load than is indicated by the theoretical calculations on which the method is based. To make an accurate experimental determination of the lift distribution on which to base the induced-angle calculations would require pressure measurements at several sections along the span, especially near the tips. An estimate can be made, however, of the possible error in the induced angles of attack given herein by comparison of the deduced slopes of the lift curve for infinite aspect ratio obtained from these tests and from the best force-test data available. Such a comparison indicates that the induced angle of attack may be approximately two-thirds of the calculated values given herein, which would mean a possible error of approximately ½° for a lift coefficient of 1.

It is evident, therefore, that the effective angles of attack are subject to a considerable error of uncertain magnitude. Approximate possible errors have been

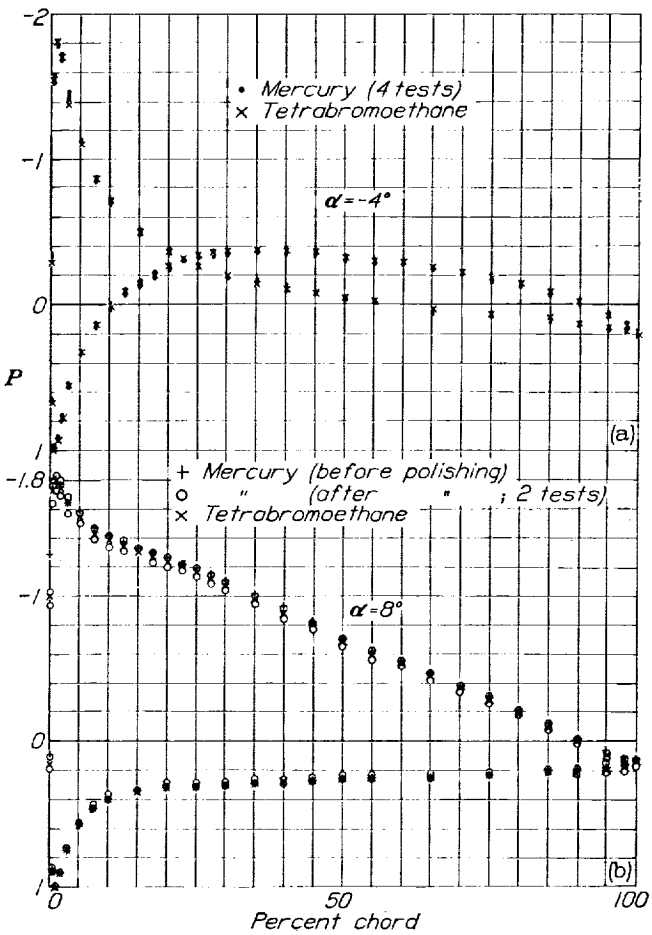

FIGURE 7.—Pressure-distribution diagrams from several tests at two angles of attack.

estimated and summarized as follows: The values of the angles as given may be too large by a constant error of approximately ¼° because of a possible error in the assumed direction of the stream. On the other hand, the angles may be too small by approximately $c_l/2°$, owing to the error in the induced-angle calculations.

THEORETICAL PRESSURE DISTRIBUTION

POTENTIAL-FLOW THEORY

A theoretical determination of the distribution of pressure about an airfoil section has been developed for potential flow and assumes an ideal fluid that is nonviscous and incompressible. Briefly, the method consists of the conformal transformation of the airfoil section into a circle. Then, inasmuch as the flow about the circle can readily be calculated, the flow characteristics about the airfoil section can be determined by means of the same transformations. References 1 and 2 present detailed discussions of the underlying theory and the derivation of the necessary equations for the calculation of the characteristics of the potential field about the airfoil.

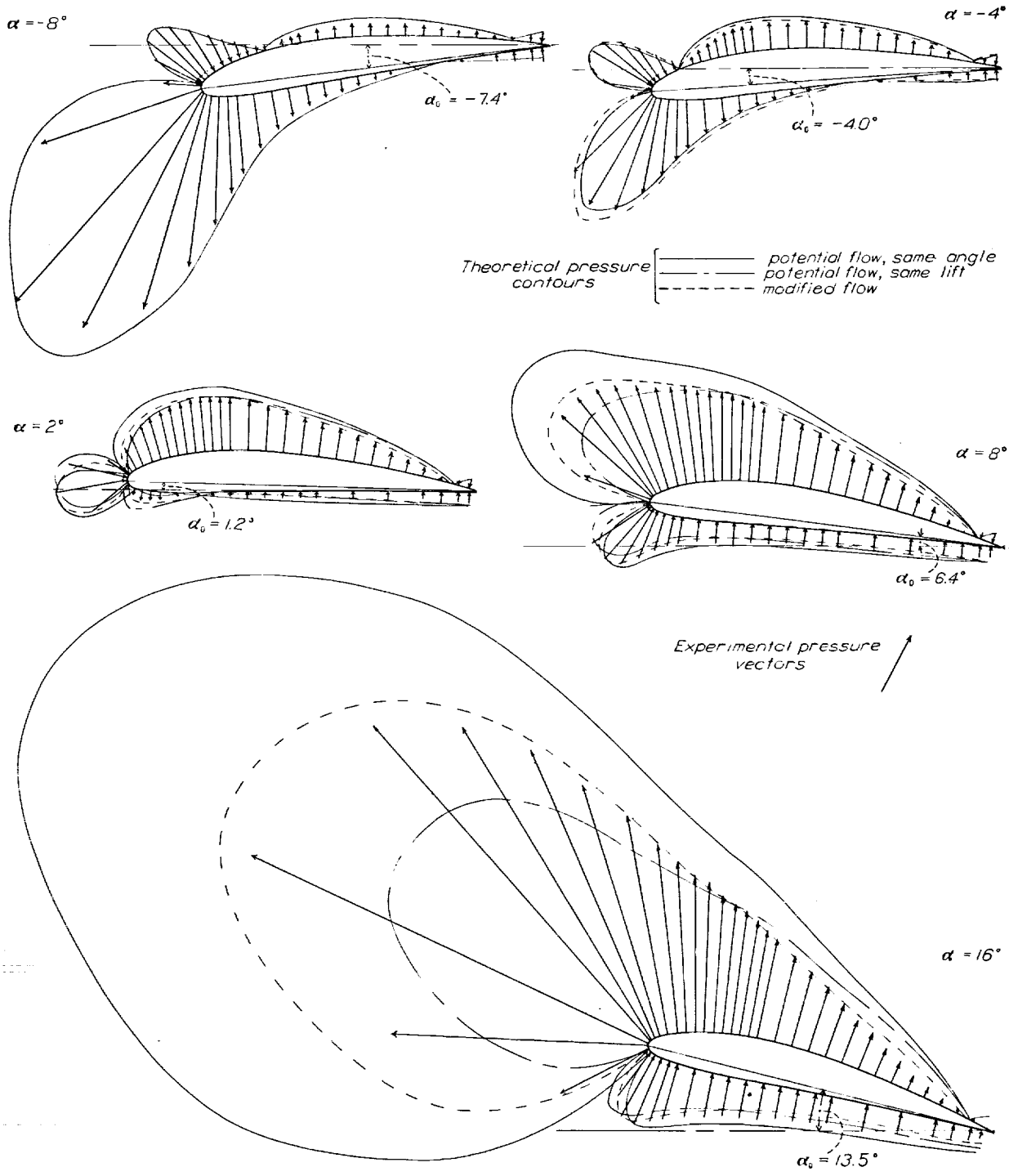

FIGURE 8.—Pressure-vector diagrams for the N. A. C. A. 4412 airfoil at several angles of attack.

The general equation for the local velocity about an airfoil section in a potential flow as given in reference 1 is

$$v = Vk\left[\sin(\theta+\epsilon+\alpha)+\frac{\Gamma}{4\pi RV}\right] \qquad (1)$$

where

$$k=\frac{\left(1+\frac{d\epsilon}{d\theta}\right)e^{\psi_0}}{\sqrt{(\sinh^2\psi+\sin^2\theta)\left[1+\left(\frac{d\psi}{d\theta}\right)^2\right]}} \tag{2}$$

V is the velocity of the undisturbed stream.

α, the angle of attack (2-dimensional).

Γ, the circulation.

θ, ψ, ϵ, parameters that are functions of the airfoil coordinates.

ψ_0, the mean value of ψ.

$R=ae^{\psi_0}$, the radius of the conformal circle about which the flow is calculable.

In order to calculate the velocity field from equation (1) the circulation must be evaluated. This evaluation is done by the use of the Kutta condition, which requires that the velocity at the trailing edge ($\theta=\pi$) be zero so that equation (1) becomes

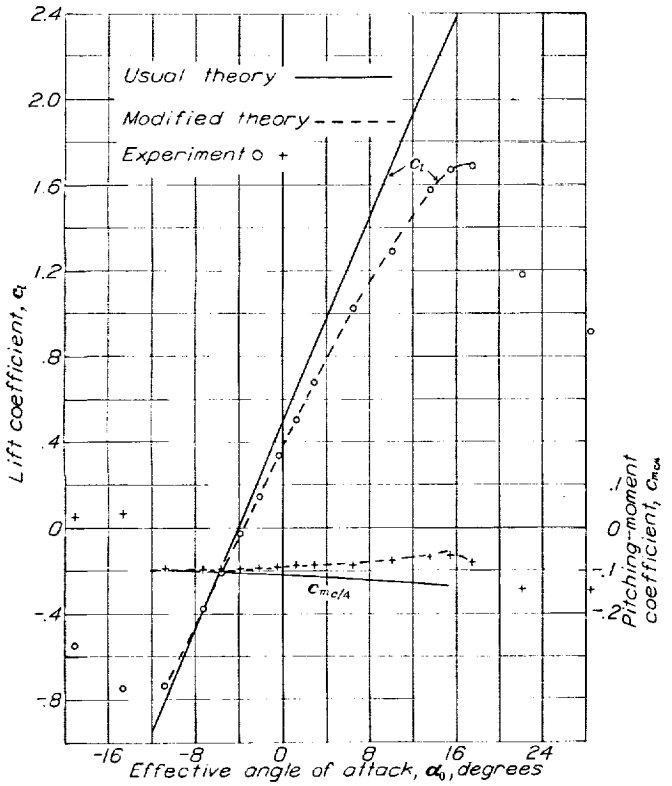

FIGURE 9.—Lift and pitching-moment section characteristics for the N. A. C. A. 4412 airfoil.

$$v=Vk[\sin(\theta+\epsilon+\alpha)+\sin(\alpha+\epsilon_T)] \tag{1a}$$

where ϵ_T is the value of ϵ at $\theta=\pi$ (trailing edge).

The angle of zero lift is equal to $-\epsilon_T$.

The necessary equations and a step-by-step description of the calculation of the velocity field are given later. The pressure coefficients are computed by means of Bernoulli's equation,

$$P=\frac{p-p_\infty}{q}=1-\left(\frac{v}{V}\right)^2 \tag{3}$$

where p is the pressure at the airfoil surface and p_∞ the pressure of the free stream.

COMPARISON OF THEORY AND EXPERIMENT

The theoretical distributions of pressure have been calculated for the 2-dimensional angles of attack corresponding to the measured distributions on the N. A. C. A. 4412 airfoil. Comparisons of the calculated and measured distributions are presented in figure 5 (excluding the diagrams after the airfoil has stalled) and in figure 8. Figure 5 presents the usual normal- and chord-component pressure diagrams and provides a means for a general study of the differences between the theory and experiment as a function of angle of attack. Figure 8 provides a more detailed study at a few angles of attack and presents vector diagrams for the angles of −8°, −4°, 2°, 8°, and 16°. These diagrams were obtained by plotting the pressure coefficients normal to the airfoil profile; the perpendicular distance from the profile line represents the magnitude of the coefficient. The experimental pressures are represented by the drawn vectors and the theoretical pressures by the solid contour line. The other contour lines represent certain modified calculations to be discussed later.

It is immediately evident that the theoretical results do not satisfactorily agree with the actual measurements except for angles of attack near −8°, corresponding approximately to the angle at which the experimental and theoretical lifts are the same (fig. 9). The comparisons in figure 5 show, moreover, that with increasing angle of attack the differences between theory and experiment become larger as predicted by the higher slope of the theoretical lift curve. A detailed study of the vector diagrams (fig. 8) shows how these differences vary around the profile of the airfoil. The largest differences occur in the regions of low pressures, or the high-velocity areas, and as previously stated they increase with increasing angle of attack. Furthermore, the percentage difference in pressure is larger near the trailing edge than in the region of the nose, indicating a progressive influence on the flow as it moves over the airfoil surface.

The effect of these differences in the pressure distribution on the pitching-moment characteristics is shown in figure 9. The theoretical pitching moment about the quarter-chord point was obtained by integrating theoretical pressure diagrams. The results show an increasing diving moment with increasing angle of attack, whereas the diving moment actually decreases.

The comparisons have thus far been made at the same relative angle of attack, that is, for the angle of attack in 2-dimensional flow. Another condition of comparison that has been used more or less regularly in previous studies is suggested; it allows a comparison at the same lift and consists in comparing the theoretical distribution calculated at an angle of attack that gives a theoretical lift equal to the experimental

value. This method has been used for the diagrams in figure 8 and the distributions thus calculated are represented thereon by the long-and-short-dash contour lines. Again the differences are too large to be neglected, especially at angles of attack where a large lift is obtained. At $-8°$ the curve coincides with the previously described contour, since the angle and the lift are the same, while at $-4°$ the distribution calculated on the basis of the same lift is approximately the same as the dashed contour representing a third calculation presented herein. At the higher angles of attack the calculated distributions depart progressively in shape from the measured distributions. It may therefore be concluded that, on the basis of these comparisons, the usual calculations from the potential theory do not give an accurate determination of the distribution of pressure about an airfoil.

The inaccurate prediction of the forces on an airfoil by the usual potential-flow theory is not surprising since the theory neglects the frictional force of the viscuous fluid acting on the airfoil. The direct effect of this force, which acts tangential to the direction of the local flow, is important only on the drag and contributes what is known as the "skin-friction" drag. Because of the small magnitude and the direction of this force, the component in the direction of the lift is probably negligible, the lift being determined entirely by the pressure forces. The indirect effect, however, of this friction force is the deceleration of the air in a thin layer near the surface of the airfoil and the production of the so-called "boundary-layer" phenomena, which are important in the development of lift by an airfoil. In the boundary layer the velocity changes rapidly from zero at the surface of the airfoil to the value of the local stream velocity at the outer limit of the layer. The loss of energy involved in overcoming the friction forces results in a cumulation of slowly moving air as the flow moves back along the airfoil; hence the boundary-layer thickness increases toward the trailing edge. This cumulative effect is indicated by the progressive increase in the differences between the theoretical and measured pressures.

From this discussion it is not to be presumed that agreement between the measured and calculated results should occur at zero lift, except approximately for a symmetrical airfoil section. The velocity distributions over the upper and lower surfaces of an asymmetrical section are not the same, even at zero lift. The viscous effects on the flow over the two surfaces at the calculated angle of zero lift are therefore different and a lift is measured, which is negative for most sections. Actually, then, the experimental and theoretical angles of zero lift are not the same and for normal sections the two lift curves intersect at a negative value of the lift coefficient.

Outside the boundary layer the viscous forces can probably be considered negligible and the flow a potential one; probably the pressures may also be considered as being transmitted undiminished through the thin boundary layer. The actual flow might therefore be replaced by a potential flow about a shape slightly different from that defined by the airfoil coordinates, which would require the determination of the boundary-layer thickness to define the effective profile shape. The pressure about the new shape could then be computed by the potential theory. Boundary-layer calculations, however, are at present subject to uncertainties that would cast doubt on the validity of the results and, in addition, the computations are difficult and tedious.

MODIFIED THEORETICAL CALCULATIONS

A simpler and more practical method of calculating the pressure over an airfoil section has been developed

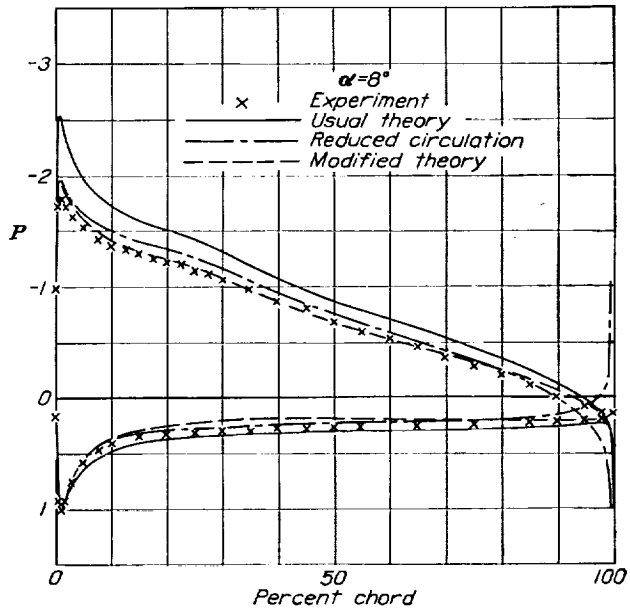

FIGURE 10.—Effect of an arbitrary reduction of the circulation on the calculated pressure distribution.

as a result of the foregoing analysis. The analysis shows that theoretical distributions calculated at the true angle of attack are similar in shape to the true distributions but give too high a lift. Conversely, when the theoretical distributions are calculated at an angle of attack that gives the same lift as the experimental distribution, the two distributions are dissimilar in shape.

The modified calculation is made at the effective angle of attack but the circulation is determined from the experimentally measured lift instead of by the Kutta-Joukowsky method. The preliminary calculations made on this basis resulted in an excessive velocity and a consequent high suction pressure at the trailing edge, as shown in figure 10. This unsatisfactory result (shown by the dot-dash line in fig. 10) was finally avoided by means of a further modification subsequently described.

Since a change in the effective profile shape has been predicted by boundary-layer considerations, an arbitrary modification of the shape parameter ϵ is made so that the velocity becomes zero at $\theta=\pi$. (See equation (1).) The shape is thus altered to satisfy again the Kutta-Joukowsky condition. In order to maintain the continuity of the ϵ curve, a study has been made of the manner in which ϵ should be modified. The indicated cumulative effects of the viscous forces toward the trailing edge show that most of the change in ϵ should probably be made in that region. Inasmuch as the effect of changing ϵ is not critical for different distributions of the change, provided that most of the change is made near the trailing edge of the airfoil, a purely arbitrary distribution is chosen that permits ready application, namely, a sinusoidal variation with θ.

The ϵ curve and subsequently the other parameters must be modified for each angle of attack. This modification has been made and the corresponding pressure distributions determined for several angles of attack. (See figs. 5 and 8.) At $-8°$ the distribution is the same as that shown by the solid line representing the unaltered theory. In the other diagrams the distributions obtained by means of the modified calculations are given by the dashed lines. The relative merit of the unaltered potential theory and the modified method for the calculation of the pressure distribution about an airfoil section is shown in figures 5, 8, and 9.

The following step-by-step description of the computations required to obtain the calculated pressure distribution is given in sufficient detail to enable the calculations for any airfoil to be made. The local velocity about the airfoil is computed by means of equation (1)

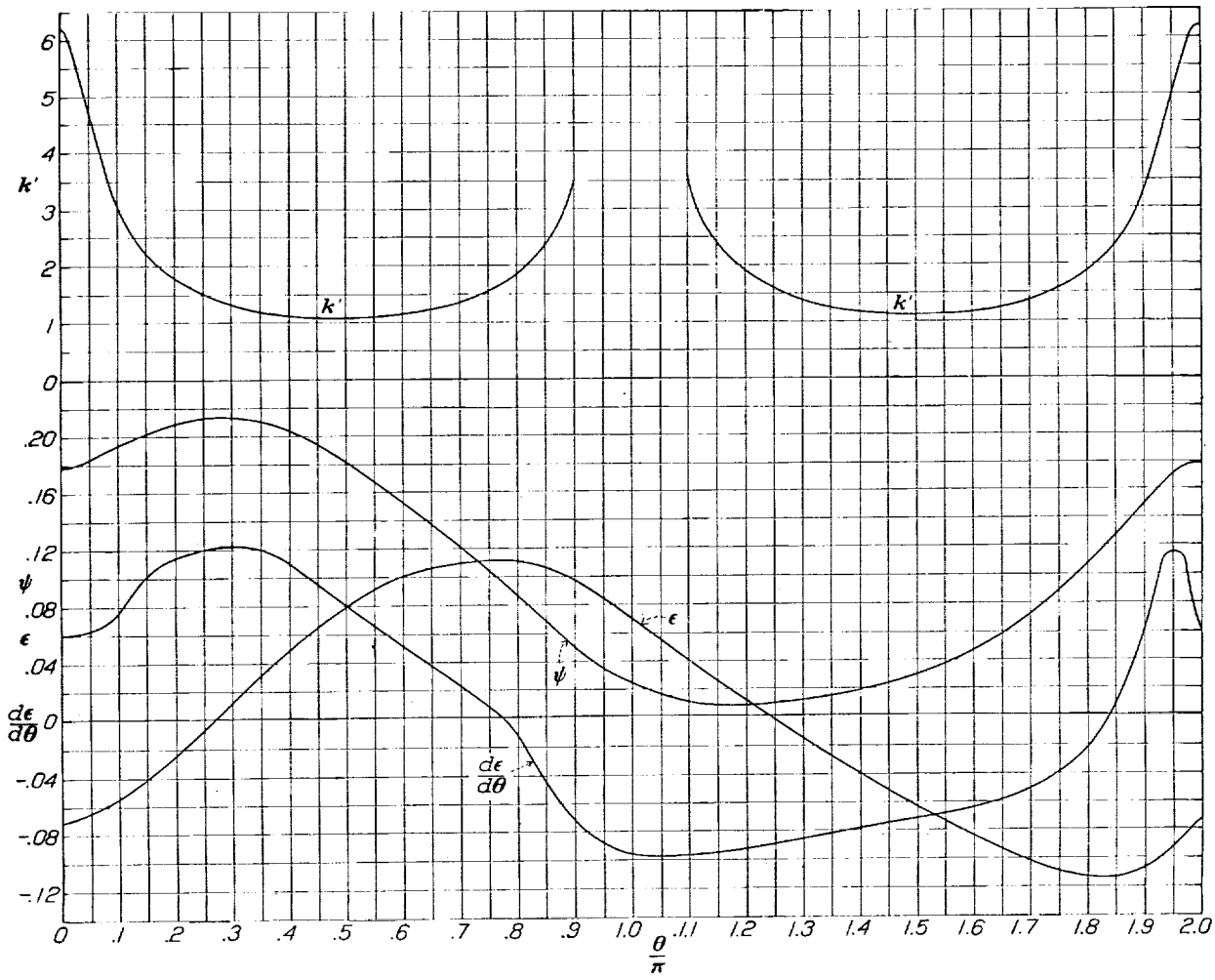

FIGURE 11.—Theoretical parameters required to compute the theoretical pressures on the N. A. C. A. 4412 airfoil.

modified as indicated by the preceding discussion. The detailed forms of the modifications are introduced as they appear in the course of routine computations.

In order that the transformation from the airfoil to its conformal circle may be of a convenient form, the coordinate axes are selected so that the profile is as nearly as possible symmetrical about them. (See reference 1.) The x axis is chosen as the line joining the centers of the leading- and trailing-edge radii. The origin is located midway between a point bisecting the distance from the leading edge to the center for the leading-edge radius and the corresponding point at the trailing edge; the coordinates of these points are

respectively $(2a, 0)$ and $(-2a, 0)$. In the following discussion the coordinate scale has been chosen so that a is unity. (For practical purposes it is probably sufficient to choose the chord joining the extremities of the mean line as the x axis.)

The following equations express the relationship between the airfoil coordinates previously described and the parameters θ and ψ.

$$\begin{aligned} x&=2\cosh\psi\cos\theta \\ y&=2\sinh\psi\sin\theta \end{aligned} \tag{4}$$

In order to compute values of θ corresponding to any given point on the airfoil profile, equations (4) are solved for $\sin^2\theta$.

$$\sin^2\theta=\frac{1}{2}(h+\sqrt{h^2+y^2}) \tag{5}$$

where

$$h=1-\left(\frac{x}{2}\right)^2-\left(\frac{y}{2}\right)^2$$

A similar solution for $\sinh^2\psi$ can be obtained but experience has shown that a more usable solution is given by the equation below

$$\sinh\psi=\frac{y}{2\sin\theta} \tag{6}$$

A plot of ψ as a function of θ for the N. A. C. A. 4412 airfoil is given in figure 11. The function ψ_0 is given by

$$\psi_0=\frac{1}{2\pi}\int_0^{2\pi}\psi d\theta$$

and can be determined graphically from the ψ curve or by a numerical evaluation. The value of ψ_0 for the N. A. C. A. 4412 airfoil is

$$\psi_0=0.1044$$

The parameter ϵ as a function of θ is given by the definite integral,

$$\epsilon_n=-\frac{1}{2\pi}\int_0^{2\pi}\psi\cot\frac{\theta-\theta_n}{2}d\theta \tag{7}$$

where the subscript n refers to the particular value of θ for which the corresponding value of ϵ is to be determined. A 20-point numerical evaluation of this integral is derived in reference 1 and is included here for convenience. The integral is evaluated at 20 equal interval values of θ, namely,

$$\begin{aligned} \theta_0&=0=\theta_{-20} \\ \theta_1&=\frac{\pi}{10}=\theta_{-19} \\ \theta_2&=\frac{2\pi}{10}=\theta_{-18} \\ &\cdots \\ \theta_{20}&=2\pi=\theta_0 \end{aligned}$$

The value of ϵ at $\theta_n=\frac{n\pi}{10}$ is given by the following equation.

$$\begin{aligned} \epsilon_n=-\frac{1}{\pi}\Big[&\frac{\pi}{10}\left(\frac{d\psi}{d\theta}\right)_n+1.091\ (\psi_{n+1}-\psi_{n-1}) \\ &+0.494\ (\psi_{n+2}-\psi_{n-2}) \\ &+0.313 \\ &+0.217 \\ &+0.158 \\ &+0.115 \\ &+0.0804 \\ &+0.0511 \\ &+0.0251\ (\psi_{n+9}-\psi_{n-9})\Big] \end{aligned} \tag{8}$$

where the subscripts designate the particular θ at which the named quantity is taken. A plot of ϵ as a function of θ for the N. A. C. A. 4412 airfoil is given in figure 11. Thus far the calculations are identical with those made for the potential theory.

As stated in the discussion of the modified theoretical calculations, the circulation is evaluated by the experimentally known lift of the airfoil section. The well-known equation relating the lift and the circulation is

$$L=\rho V\Gamma$$

Also by definition

$$L=\frac{1}{2}\rho V^2 c c_l$$

Expressing the circulation in terms of the lift coefficient,

$$\Gamma=\frac{cV}{2}c_l$$

and finally

$$\frac{\Gamma}{4\pi RV}=\frac{c}{8\pi R}c_l \tag{9}$$

Substituting the numerical values for the N. A. C. A. 4412,

$$\frac{\Gamma}{4\pi RV}=\frac{1}{6.915}c_l \tag{9a}$$

The prediction of unreasonable velocities around the trailing edge is avoided by altering the ϵ function so that the velocity is zero at $\theta=\pi$. The altered function is designated ϵ_α and is arbitrarily assumed to be given by

$$\epsilon_\alpha=\epsilon+\frac{\Delta\epsilon_T}{2}(1-\cos\theta) \tag{10}$$

where $\Delta\epsilon_T$ is the increment of ϵ required to give zero velocity at $\theta=\pi$ and is a function of the angle of attack. The quantity $\Delta\epsilon_T$ is given by

$$\Delta\epsilon_T=\epsilon_{\alpha_T}-\epsilon_T$$

where ϵ_{α_T} is determined by equating equation (1) to zero and substituting from equation (9).

$$\sin(\pi+\alpha+\epsilon_{\alpha_T})+\frac{c}{8\pi R}c_l=0$$

Solving for ϵ_{α_T} gives,

$$\epsilon_{\alpha_T}=\sin^{-1}\frac{c}{8\pi R}c_l-\alpha$$

The parameters ϵ and ψ are conjugate functions of θ, and ψ is given by

$$\psi_n=\frac{1}{2\pi}\int_0^{2\pi}\epsilon\cot\frac{\theta-\theta_n}{2}d\theta+\psi_0$$

where the definite integral can be evaluated in the same manner as equation (7). The coordinates of the profile corresponding to the modified ϵ function can be obtained from the new ψ function by equations (4). Figure 12 gives the modified shape obtained by this method for the N. A. C. A. 4412 airfoil at $\alpha=8°$ and 16°.

The profiles given in figure 12 are, of course, only effective profiles corresponding to the calculations. The actual profile about which a potential flow might be considered as being established would be blunt at the trailing edge and would have the thickness of the wake at that point. The thickness of the boundary layer on the upper surface, however, is greater than that on the lower surface; therefore, if the trailing edge were taken as the midpoint of the wake and the after portion of the profile were faired to that point, the

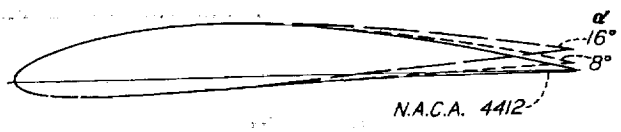

FIGURE 12.—Change in profile shape associated with the modified theoretical calculation of pressure.

resulting shape would be similar to the effective profiles in figure 12.

The influence of the changes in ψ on the value of k are found to be negligible so that k_α may be written

$$k_\alpha=\left(1+\frac{d\epsilon_\alpha}{d\theta}\right)k'$$

where

$$k'=\frac{e^{\psi_0}}{\sqrt{(\sinh^2\psi+\sin^2\theta)\left[1+\left(\frac{d\psi}{d\theta}\right)^2\right]}}$$

Differentiating equation (10)

$$\frac{d\epsilon_\alpha}{d\theta}=\frac{d\epsilon}{d\theta}+\frac{\Delta\epsilon_T}{2}\sin\theta$$

Plots of $\frac{d\epsilon}{d\theta}$ and k' as functions of θ for the N. A. C. A. 4412 airfoil are given in figure 11. Equation (1) for the velocity at any point on the airfoil profile is now written

$$v=Vk_\alpha\left[\sin(\theta+\epsilon_\alpha+\alpha)+\frac{c}{8\pi R}c_l\right] \qquad (1b)$$

The generality of the preceding method of calculating the pressure distribution about an airfoil section is supported by the following evidence. First, no restricting assumptions have been made in the development of the method. Second, the circulation is determined by a known quantity, the experimentally measured lift. Third, the change in the effective airfoil shape is in the direction indicated by boundary-layer considerations. Finally, the computed and measured pressures agree satisfactorily.

LANGLEY MEMORIAL AERONAUTICAL LABORATORY,
NATIONAL ADVISORY COMMITTEE FOR AERONAUTICS,
LANGLEY FIELD, VA., *March 25, 1936.*

REFERENCES

1. Theodorsen, T., and Garrick, I. E.: General Potential Theory of Arbitrary Wing Sections. T. R. No. 452, N. A. C. A. 1933.
2. Theodorsen, Theodore: Theory of Wing Sections of Arbitrary Shape. T. R. No. 411, N. A. C. A., 1931.
3. Jacobs, Eastman N., and Abbott, Ira H.: The N. A. C. A. Variable-Density Wind Tunnel. T. R. No. 416, N. A. C. A., 1932.
4. Millikan, Clark B.: On the Lift Distribution for a Wing of Arbitrary Plan Form in a Circular Wind Tunnel. Publication No. 22, C. I. T., 1932.

TABLE I.—EXPERIMENTAL DATA—N. A. C. A. 4412 AIRFOIL

[Average pressure (standard atmospheres): 21; average Reynolds Number: 3,100,000]

Orifices			Values of pressure coefficient, $P=\frac{p-p_\infty}{q}$, for different angles of attack															
Designation	Station (percent c from L. E. of chord)	Ordinate (percent c above chord)	−20° [1]	−16° [1]	−12° [1]	−8° [1]	−6° [2]	−4° [2]	−2° [2]	0° [2]	2° [2]	4° [2]	8° [2]	12° [1]	16° [1]	18° [1]	20° [1]	24° [1]	30° [1]
28	100.00	0	−0.421	−0.199	0.114	0.198	0.217	0.204	0.207	0.200	0.181	0.158	0.134	0.101	0.010	−0.062	−0.173	−0.466	−0.513
1	97.92	−.16	−.454	−.251	.159	.224	.181	.178	.180	.183	.164	.157	.167	.140	.121	.094	.049	−.291	−.304
29	94.86	−.16	−.466	−.291	.107	.185	1.52	.151	.158	.166	.154	.156	.180	.166	.179	.166	.127	−.160	−.167
2	89.90	−.22	−.505	−.330	.074	.153	.122	.128	.140	.156	.152	.160	.203	.199	.231	.237	.224	−.030	−.036
30	84.94	−.28	−.538	−.382	.035	.107	.072	.082	.098	.118	.118	.158	.211	.212	.257	.270	.283	.049	.042
31	74.92	−.52	−.558	−.454	−.043	.055	.049	.068	.095	.126	.136	.158	.231	.251	.322	.348	.374	.179	.179
32	64.94	−.84	−.564	−.539	−.101	.002	.000	.028	.062	.104	.120	.154	.244	.283	.374	.407	.453	.270	.289
3	54.48	−1.24	−.571	−.643	−.199	−.082	−.063	−.024	.021	.072	.100	.157	.250	.309	.414	.452	.492	.348	.368
33	49.98	−1.44	−.571	−.695	−.252	−.115	−.099	−.053	−.005	.050	.091	.134	.252	.316	.426	.472	.531	.381	.407
4	44.90	−1.64	−.571	−.721	−.304	−.160	−.128	−.075	−.017	.048	.088	.140	.268	.342	.459	.505	.570	.413	.446
34	39.98	−1.86	−.558	−.754	−.368	−.206	−.169	−.105	−.041	.031	.071	.136	.265	.362	.485	.544	.609	.466	.498
5	34.90	−2.10	−.551	−.773	−.447	−.258	−.217	−.146	−.073	.010	.066	.133	.290	.387	.516	.576	.642	.504	.544
35	29.96	−2.30	−.545	−.786	−.545	−.330	−.274	−.190	−.105	−.011	.048	.116	.293	.414	.551	.609	.687	.557	.596
6	24.90	−2.54	−.545	−.806	−.688	−.427	−.367	−.266	−.165	−.054	.025	.115	.313	.433	.589	.661	.726	.609	.648
36	19.98	−2.76	−.551	−.819	−.896	−.591	−.490	−.365	−.244	−.111	−.011	.093	.321	.472	.627	.687	.752	.642	.700
7	14.94	−2.90	−.558	−.825	−1.178	−.799	−.663	−.502	−.348	−.180	−.053	.076	.345	.518	.713	.785	.857	.733	.778
37	9.96	−2.86	−.551	−.832	−1.660	−1.143	−.946	−.716	−.501	−.279	−.111	.059	.402	.616	.818	.883	.948	.824	.876
8	7.38	−2.72	−.577	−.916	−2.070	−1.407	−1.153	−.867	−.596	−.333	−.131	.071	.462	.713	.896	.961	1.019	.902	.941
38	4.94	−2.46	−.571	−.897	−2.807	−1.861	−1.490	−1.106	−.777	−.428	−.150	.109	.568	.818	.980	1.013	1.046	.948	.980
9	2.92	−2.06	−.702	−1.242	−3.745	−2.468	−1.931	−1.380	−.932	−.467	−.098	.231	.748	.948	.993	.948	.909	.883	.941
39	1.66	−1.60	−1.053	−1.947	−4.940	−3.198	−2.478	−1.709	−1.059	−.436	.028	.409	.916	.974	.791	.596	.433	.602	.713
10	.92	−1.20	−2.082	−3.212	−6.177	−3.770	−2.765	−1.812	−.995	−.266	.254	.643	1.013	.831	.264	−.173	−.518	.003	.244
40	.36	−.70	−3.204	−4.300	−7.337	−4.052	−2.732	−1.559	−.631	.156	.639	.924	.905	.094	−1.379	−2.285	−3.012	−1.671	−1.059
11	0	0	−2.623	−3.433	−5.480	−2.397	−1.232	−.296	.356	.834	.989	.952	.157	−1.555	−3.648	−5.060	−6.073	−3.695	−2.382
41	0	.68	−1.178	−1.549	−2.625	−.538	.184	.681	.945	1.010	.854	.473	−1.000	−3.250	−6.230	−7.775	−8.941	−5.660	−3.730
12	.44	1.56	.322	.231	−.043	.765	.955	.994	.948	.720	.336	−.202	−1.740	−3.738	−5.961	−7.125	−7.954	−4.698	−2.552
42	.94	2.16	.739	.720	.596	.974	1.009	.939	.770	.468	.055	−.456	−1.793	−3.399	−5.210	−6.110	−6.681	−3.881	−2.006
13	1.70	2.78	.928	.935	.883	1.000	.939	.782	.569	.246	−.148	−.611	−1.743	−3.053	−4.478	−5.190	−5.620	−3.010	−1.249
43	2.94	3.64	.987	1.000	.974	.896	.761	.559	.332	.018	−.336	−.728	−1.647	−2.637	−3.765	−4.285	−4.562	−2.200	−.786
14	4.90	4.68	.922	.935	.896	.713	.542	.333	.110	−.179	−.485	−.813	−1.547	−2.343	−3.190	−3.570	−3.731	−1.529	−.695
44	7.50	5.74	.804	.798	.752	.498	.344	.139	−.066	−.312	−.568	−.831	−1.432	−2.057	−2.709	−2.981	−3.060	−1.235	−.644
15	9.96	6.56	.687	.687	.622	.374	.208	.017	−.168	−.388	−.623	−.872	−1.391	−1.912	−2.440	−2.662	−2.681	−1.059	−.630
45	12.58	7.34	.583	.576	.498	.263	.089	−.091	−.271	−.468	−.676	−.899	−1.350	−1.802	−2.240	−2.415	−2.382	−1.007	−.611
16	14.92	7.88	.498	.485	.407	.178	.014	−.152	−.309	−.500	−.700	−.912	−1.308	−1.769	−2.149	−2.285	−2.180	−.955	−.604
46	17.44	8.40	.414	.407	.329	.100	−.052	−.210	−.360	−.537	−.721	−.910	−1.272	−1.620	−1.952	−2.062	−1.984	−.910	−.604
17	19.96	8.80	.335	.335	.257	.036	−.111	−.262	−.402	−.568	−.740	−.914	−1.239	−1.548	−1.841	−1.927	−1.815	−.870	−.598
47	22.44	9.16	.263	.257	.172	−.024	−.176	−.322	−.452	−.609	−.769	−.930	−1.224	−1.502	−1.758	−1.822	−1.685	−.851	−.591
18	24.92	9.52	.212	.211	.140	−.063	−.196	−.332	−.454	−.599	−.746	−.895	−1.163	−1.418	−1.640	−1.692	−1.592	−.825	−.591
48	27.44	9.62	.166	.165	.100	−.096	−.228	−.355	−.471	−.606	−.742	−.881	−1.122	−1.347	−1.535	−1.573	−1.391	−.812	−.591
19	29.88	9.76	.114	.133	.068	−.114	−.241	−.364	−.469	−.594	−.722	−.851	−1.071	−1.280	−1.438	−1.463	−1.254	−.786	−.591
49	34.98	9.90	.036	.055	.009	−.154	−.275	−.381	−.473	−.596	−.693	−.804	−.982	−1.144	−1.269	−1.255	−1.005	−.760	−.591
20	39.90	9.84	−.017	.009	−.030	−.173	−.272	−.370	−.447	−.542	−.635	−.732	−.880	−1.007	−1.099	−1.059	−.798	−.727	−.584
50	44.80	9.64	−.095	−.044	−.069	−.194	−.291	−.371	−.439	−.519	−.639	−.691	−.809	−.902	−.961	−.910	−.655	−.720	−.591
21	49.92	9.22	−.121	−.056	−.075	−.173	−.256	−.329	−.389	−.455	−.525	−.595	−.690	−.759	−.786	−.734	−.538	−.715	−.591
51	54.92	8.76	−.147	−.069	−.075	−.161	−.238	−.303	−.351	−.406	−.471	−.527	−.601	−.649	−.649	−.584	−.473	−.700	−.591
22	59.94	8.16	−.199	−.101	−.095	−.161	−.244	−.298	−.342	−.391	−.438	−.487	−.541	−.576	−.551	−.460	−.414	−.695	−.591
52	64.90	7.54	−.225	−.108	−.082	−.128	−.214	−.264	−.296	−.334	−.378	−.421	−.456	−.460	−.414	−.343	−.369	−.688	−.591
23	69.86	6.76	−.252	−.121	−.082	−.115	−.181	−.225	−.250	−.282	−.319	−.351	−.371	−.375	−.316	−.264	−.337	−.682	−.584
24	74.90	5.88	−.277	−.128	−.056	−.082	−.148	−.183	−.200	−.222	−.252	−.279	−.285	−.264	−.212	−.212	−.310	−.655	−.584
53	79.92	4.92	−.297	−.147	−.069	−.076	−.115	−.144	−.155	−.169	−.191	−.210	−.199	−.180	−.147	−.173	−.291	−.642	−.578
25	84.88	3.88	−.330	−.154	−.024	−.024	−.068	−.091	−.094	−.101	−.116	−.113	−.106	−.082	−.082	−.140	−.271	−.604	−.565
54	89.88	2.74	−.356	−.161	.022	.028	−.006	−.019	−.016	−.017	−.026	−.032	−.009	−.004	−.043	−.114	−.246	−.565	−.552
26	94.90	1.48	−.388	−.174	.075	.100	.073	.069	.078	.082	.076	.070	.079	.062	−.016	−.095	−.226	−.519	−.519
27	98.00	.68	−.434	−.200	.127	.165	.141	.139	.147	.150	.143	.127	.120	.088	−.004	−.075	−.200	−.479	−.506
28	100.00	0																	

[1] Test, variable-density tunnel 1098; manometer liquid, mercury.

[2] Test, variable-density tunnel 1099-4; manometer liquid, tetrabromoethane.

TABLE II.—INTEGRATED AND DERIVED CHARACTERISTICS—N. A. C. A. 4412 AIRFOIL

α	c_n	c_c	$c_{m_{c/4}}$	c_l	α_i	α_0
Degrees					*Degrees*	*Degrees*
−20	−0.592	0.0318	0.030	−0.545	−0.9	−19.1
−16	−.767	−.0170	.035	−.742	−1.2	−14.8
−12	−.722	−.1264	−.092	−.732	−1.2	−10.8
−8	−.372	−.0445	−.096	−.374	−.6	−7.4
−6	−.210	−.0151	−.096	−.211	−.3	−5.7
−4	−.0256	.0043	−.095	−.0255	−.0	−4.0
−2	.146	.0107	−.092	.146	.2	−2.2
0	.338	.0098	−.091	.338	.5	−.5
2	.501	−.0034	−.087	.501	.8	1.2
4	.677	−.0258	−.087	.677	1.1	2.9
8	1.020	−.1003	−.084	1.024	1.6	6.4
12	1.275	−.2043	−.074	1.289	2.0	10.0
16	1.548	−.3357	−.068	1.579	2.5	13.5
18	1.626	−.4040	−.063	1.671	2.6	15.4
20	1.640	−.4374	−.080	1.690	2.7	17.3
24	1.212	−.1838	−.141	1.182	1.9	22.1
30	1.009	−.0776	−.146	.913	1.4	28.6

TABLE III.—THEORETICAL PARAMETERS—N. A. C. A. 4412 AIRFOIL

Station (percent c)	Ordinate (percent c)	x	y	$\frac{\theta}{\pi}$	ψ	$\theta+\epsilon$	Ordinate (percent c)	x	y	$\frac{\theta}{\pi}$	ψ	$\theta+\epsilon$
Upper surface							Lower surface					
						deg. min.						deg. min.
------	------	2.032	0	0	0.178	−4 10	------	2.032	0	0	0.178	−4 10
0	0.62	2.031	.0121	.007	------	−2 4	0	2.031	−.0129	−.012	------	−6 20
.25	1.25	2.021	.0375	.034	------	2 1	−.60	2.021	−.0371	−.034	------	−10 49
.5	1.64	2.011	.0532	.046	------	4 35	−.88	2.011	−.0484	−.043	------	−12 52
1.25	2.44	1.981	.0855	.073	.186	9 48	−1.43	1.980	−.0706	−.069	.162	−18 1
2.5	3.39	1.931	.1239	.103	.194	15 29	−1.95	1.930	−.0916	−.098	.151	−23 48
5	4.73	1.830	.1784	.146	.201	23 48	−2.49	1.829	−.1130	−.140	.133	−31 47
7.5	5.76	1.730	.2203	.179	.205	30 19	−2.74	1.729	−.1227	−.172	.119	−37 39
10	6.59	1.629	.2542	.207	.208	35 58	−2.86	1.628	−.1271	−.200	.108	−42 36
15	7.89	1.427	.3075	.254	.213	45 25	−2.88	1.426	−.1271	−.249	.090	−51 11
20	8.80	1.225	.3446	.296	.213	53 56	−2.74	1.224	−.1210	−.292	.076	−58 32
25	9.41	1.024	.3696	.333	.211	61 26	−2.50	1.023	−.1110	−.330	.064	−65 2
30	9.76	.824	.3845	.369	.208	68 32	−2.26	.820	−.1005	−.366	.055	−71 6
40	9.80	.418	.3873	.435	.197	81 42	−1.80	.417	−.0807	−.435	.041	−82 47
50	9.19	.0149	.3640	.500	.181	94 32	−1.40	.0137	−.0633	−.500	.030	−93 45
60	8.14	−.389	.3229	.560	.163	106 11	−1.00	−.390	−.0460	−.560	.023	−103 50
70	6.69	−.792	.2655	.628	.143	119 0	−.65	−.793	−.0307	−.629	.017	−115 12
80	4.89	−1.196	.1940	.702	.121	132 48	−.39	−1.197	−.0190	−.704	.012	−127 32
85	3.83	−1.398	.1518	.745	.106	140 32	−.30	−1.398	−.0149	−.746	.010	−134 28
90	2.71	−1.600	.1074	.793	.089	149 23	−.22	−1.600	−.0109	−.795	.009	−142 25
95	1.47	−1.802	.0577	.855	.065	159 56	−.16	−1.802	−.0081	−.856	.009	−152 31
98	.68	−1.924	.0262	.910	.047	169 18	−.14	−1.924	−.0069	−.912	.012	−161 34
100	.13	−2.003	0	1.000	.025	184 3	−.13	−2.003	−.0013	−1.000	.025	−175 57

TABLE IV.—THEORETICAL PARAMETERS—N. A. C. A. 4412 AIRFOIL

$\frac{\theta}{\pi}$	ψ	$\frac{d\psi}{d\theta}$	k'	ϵ	$\frac{d\epsilon}{d\theta}$
0	0.1780	0	6.201	−0.0727	0.0600
.1	.1924	.0611	3.041	−.0548	.0755
.2	.2082	.0395	1.777	−.0258	.1135
.3	.2128	−.0116	1.326	.0120	.1220
.4	.2035	−.0527	1.139	.0492	.1095
.5	.1806	−.0866	1.088	.0797	.0800
.6	.1519	−.0942	1.147	.1002	.0515
.7	.1214	−.1028	1.350	.1087	.0230
.8	.0863	−.1166	1.856	.1109	−.0130
.9	.0501	−.1016	3.528	.0975	−.0720
1.0	.0250	−.0590	-------	.0706	−.0960
1.1	.0118	−.0249	3.589	.0403	−.0970
1.2	.0088	.0020	1.887	.0115	−.0925
1.3	.0120	.0169	1.372	−.0153	−.0860
1.4	.0192	.0284	1.167	−.0385	−.0785
1.5	.0302	.0434	1.109	−.0612	−.0720
1.6	.0470	.0661	1.163	−.0837	−.0640
1.7	.0736	.0976	1.391	−.1029	−.0505
1.8	.1080	.1211	1.845	−.1126	−.0210
1.9	.1488	.1361	3.205	−.1070	.0640
2.0	.1780	0	6.201	−.0727	.0600